Engineering Structures 212 (2020) 110504

Contents lists available at ScienceDirect

Engineering Structures

journal homepage: www.elsevier.com/locate/engstruct

Parametric 3D finite element analysis of FRCM-confined RC columns under eccentric loading

Akram Jawdhari[a,d,*], Ali Hadi Adheem[b], Majid M.A. Kadhim[c]

[a] Department of Construction and Projects, University of Babylon, Hilla, Iraq
[b] Kerbala Technical Institute, Al-Furat Al-Awsat Technical University, 56001 Kerbala, Iraq
[c] College of Engineering, University of Babylon, Hilla, Iraq
[d] Department of Civil Engineering, Queen's University, Kingston, Canada

ARTICLE INFO

Keywords:
Confinement
Eccentricity
Finite element
FRCM
RC columns
Slenderness

ABSTRACT

Fiber reinforced cementitious matrix (FRCM) is emerging as a viable retrofit and confinement technique, in lieu of fiber reinforced polymer (FRP) system which suffers from a number of issues related to the use of synthetic binders. While many studies have been conducted on the use of FRCM in shear and flexural applications, few were dedicated to confinement of slender columns, particularly those related to finite element (FE) analysis. In this study, a nonlinear three-dimensional FE model has been developed to study the behavior of reinforced concrete (RC) columns confined by (FRCM) jackets, and loaded concentrically and eccentrically. Drucker-Prager (DP) concrete model, which has several improvements over traditional DP models, was used to model the concrete core. Composite failure in the fibers comprising FRCM system and column buckling were also considered in the developed FE model. The model was validated by comparing its predictions with those of three control and 8 FRCM-confined RC columns from literature. Consequently, a parametric study utilizing 96 additional models, was performed on five parameters, namely: cross-sectional shape (square, circle, hexagon, and octagon), and for rectangular columns; aspect (h/b) ranging from 0.5 to 3, at 0.5 increment; slenderness (KL/r) ratio, considering four values, 10, 25, 50, and 75; load eccentricity (e) as a ratio (e/h) to side length (h), varying from 0 to 2.5; and concrete compressive strength ($\acute{f}_c$), studying three values: 20, 35, and 50 MPa. Effects of these parameters on the column's maximum load (P_{max}) and general behavior, are discussed in details in Section 6 and summarised in the conclusions part. In general, P_{max} increased by 0–32% as a result of applying one layer of FRCM jacket, and showed great dependence on the examined parameters.

1. Introduction

Reinforced concrete structures are facing a major deterioration problem globally due to aging; exposure to environmental conditions such as freeze-thaw cycles, moisture, de-icing agents; lack of maintenance; etc. [1,2]. The use of fiber reinforced polymer (FRP) composites has gained considerable popularity due to their favorable properties, including low weight-to-strength ratio, ease of application, corrosion resistance, and minimal change in structure's geometry [3–5]. In concrete retrofit applications, FRP reinforcement is typically applied as an externally bonded (EB) or as near surface mounted (NSM), both are installed using organic adhesives such as epoxy [1,7]. Epoxy-bonded FRP strengthening techniques have some drawbacks, including: inapplicability on wet surface or at low temperature, high cost, poor performance under high temperature and lack of vapor permeability [1,7].

In order to overcome these issues, researchers examined the replacement of epoxy resins with inorganic (cement mortar) matrix [1,6–11]. The mortar can be used to bond EB FRP and NSM FRP reinforcements, but it's generally more effective with fabric meshes and grids — resulting in a retrofit system known in literature as fiber-reinforced cementitious matrix (FRCM) [7]. Different types of fibers, such as carbon, glass, basalt, or Polyparaphenylene Benzobisoxazole (PBO), can be used in fabricating the FRP mesh/grid [10] in FRCM technique. Several tests have been performed to validate the effectiveness of FRCM system in strengthening concrete and masonry members against shear, flexure, and torsion, with results showing significant increase in load capacity and reduction in deflections and crack widths, in addition to improved behavior under elevated temperatures or in fire [6,7,9–14].

Research on strengthening or confinement of axial RC members using FRCM technique can also be found in literature, although in smaller numbers than other applications [15–20]. Available studies can

* Corresponding author.
E-mail addresses: akram.hassan@uky.edu (A. Jawdhari), inkr.ali@atu.edu.iq (A.H. Adheem), eng.majid.mohammed@uobabylon.edu.iq (M.M.A. Kadhim).

https://doi.org/10.1016/j.engstruct.2020.110504
Received 20 August 2019; Received in revised form 2 February 2020; Accepted 9 March 2020

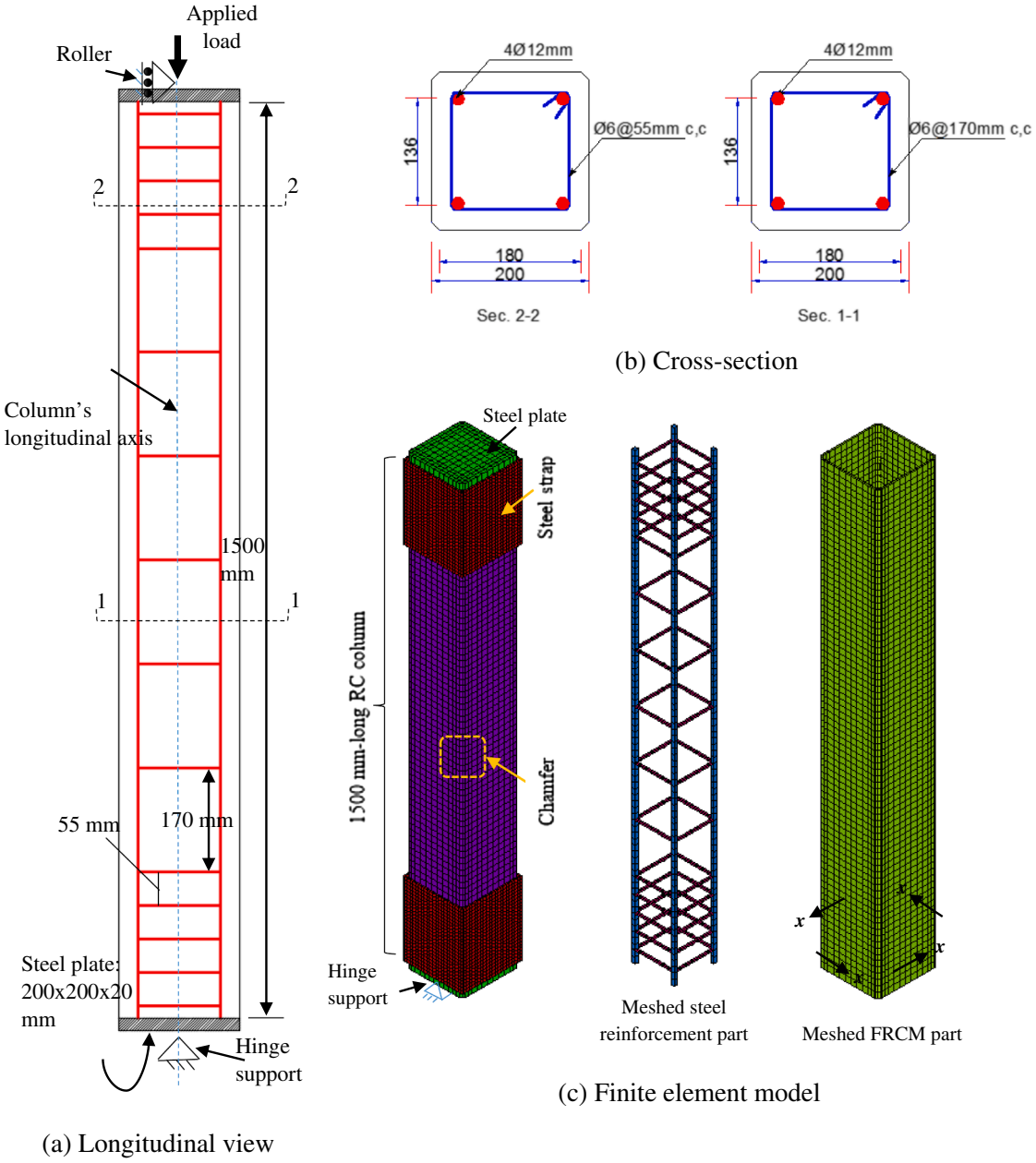

Fig. 1. Geometry of FRCM jacketed RC columns, and FE model.

be divided into two main categories: short (plain) concrete columns such as [15–17] and slender reinforced concrete columns [18–20]. Variables investigated ranged from material related ones (concrete strength, fiber type), geometrical related ones (length and cross-section), and eccentricity of axial load. It was found that the FRCM jacketing had a significant contribution to improving strength and deformability of the tested samples.

However, research on FRCM-confined slender RC columns is very limited. To the authors' best knowledge, the studies by Trapko [18,19] and by Ombres and Verre [20] were the only ones found in the literature on this topic. Trapko [18,19] tested 15, 1500 mm-long square RC columns under concentric and eccentric axial load. Three specimens were un-strengthened, while the remaining 12 were strengthened with FCRM jackets having different number of layers and orientations. Two eccentricities (e) were examined, namely 16 and 32 mm, corresponding to an eccentricity-to-height (h) (e/h) ratio of 0.080 and 0.16, respectively. Results showed an increase of ultimate load ($P_{ult.}$) by 13.5, 17.7, and 4.7% relative to the control columns, when one transverse layer, two transverse layers, and one transverse combined with one longitudinal layers of FRCM were used, respectively. However, $P_{ult.}$ decreased in average by 11 and 31%, when the eccentricity increased from 0 to 16 and 32 mm, respectively.

Ombres and Verre [20] tested eight slender RC columns, confined by FRCM technique. The variables examined were: eccentricity(e/h) ratio from 0 to 0.33; and number of FRCM layers, varying from one to two. The results were similar to those observed by Trapko [18–19] where the increase in ultimate load for FRCM-strengthened columns varied between 20% and 39%. In addition, it was found that the strength gain was inversely proportional to the eccentricity value. Given the small number of studies and limited parameters examined, further research on FRCM-confined RC columns is warranted. In addition, there is no finite element (FE) study performed on this research topic.

Validated FE models can be powerful analytical tool, where it typically results in tremendous reductions of time and cost, compared to experimental tests. Several studies utilized FE analysis in studying the behavior of RC members strengthened with FRCM, focusing on flexural,

torsional, and bond aspects [21–24]. For example, Alabdulhady et al. [21] developed an LS DYNA FE model to study the behavior of FRCM-strengthened RC beams under torsion and reported a good match between experimental and numerical results. Kadhim et al. [24] used ANSYS software to develop a FE model, studying the response of RC beams strengthened in shear with FRCM wraps and concluded of good calibration between numerical and test data.

2. Significance and objectives

In many instances, axial concrete members sustain damage due to impact or seismic activity and therefore require rehabilitation and upgrade, conventionally by FRP sheets and wraps. FRCM technique provides the advantages of conventional FRP systems, while minimizing the problems related to organic adhesive. The effectiveness of FRCM technique in confining or strengthening RC columns, especially slender ones, has not been fully examined and understood. The objective of this paper is to develop and validate a robust, non-linear finite element (FE) model, capable of predicting the behavior of FRCM-confined RC columns. The model predictions were validated mainly by comparing with 11 tests performed on long, square RC columns wrapped with FRCM jackets, and loaded concentrically and eccentrically. To provide further fidelity, particularly for different cross-sectional shapes, the model was used to replicate three circular concrete cylinders confined by FRCM jackets.

The validated model is used mainly to examine a wide range of parameters that have not been studied yet, including: (a) the aspect ratio of rectangular column (h/b), ranging from 0.5 to 3; (b) column's cross-section shape using circle, square, hexagon, and octagon; (c) slenderness (KL/r) ratio, ranging from 10 to 75; concrete compressive strength ($\acute{f}_c$), studying three values 20, 35, and 50 MPa; and load eccentricity (e/h) ratio, ranging from 0 to 2.5. It should be noticed that (e/h) ratios exceeding 0.5 correspond to loads outside the concrete section, for which experimental observation can be extremely difficult.

2.1. Summary of tests

The RC concrete columns tested by Trapko [18,19] were selected to validate the predictions of the FE model developed in this study. These columns were 1500 mm long, and had a square cross-section of $b \times h = 200 \times 200$ mm, Fig. 1(a and b). In total, 15 specimens were tested, including three un-strengthened (control) and twelve strengthened by FRCM, consisting of PBO fabric mesh embedded in a cementitious mortar. The fabric was in the form of unbalanced net, with rovings spaced at 10 and 20 mm, in the longitudinal and transverse directions, respectively. The thickness of an equivalent continuous fabric, idealized by distributing the fibers evenly over the entire mesh width, was 0.046 and 0.012 mm for the above respective directions.

The variables investigated were load eccentricity (e), and number of layers for FRCM and its configuration. For eccentricity, three values were examined, namely: $e = 0$ (concentric load), $e = 16$ mm, and $e = 32$ mm; corresponding to an eccentricity-to-height (h) (e/h) ratio of 0, 0.08 and 0.16, respectively. Strengthened columns were those confined by either: one layer of horizontal [i.e. longitudinal fibers are oriented parallel to x-axis in Fig. 1(c)] FRCM; two layers of horizontal FRCM; one vertical [i.e. longitudinal fibers are oriented parallel to column's length] and one horizontal layers of FRCM; and one vertical and two horizontal layers of FRCM, see Table 1.

From the tested samples, 11 columns were selected for modeling, including 3 control ones and 8 FRCM-confined ones. The test matrix, including examined parameters and key results of the modeled columns, is shown in Table 1. The specimen code defined in the experiments [18,19] is as following; C_XY_ZM_E, where C is constant for all columns and refers to "column"; X is number of layers for first applied mesh; Y is orientation of first mesh (either horizontal "H" or vertical "V"); Z is number of layers for subsequent meshes; M is orientation of subsequent meshes (either horizontal "H" or vertical "V"); E is eccentricity in millimeters. The nominal compressive ($f_{c'}$) strength of the concrete core and cementitious mortar were 49, 29 MPa, respectively. The longitudinal steel reinforcement consisted of four 12 mm deformed bars with a yield stress (f_y) of 500 MPa. Steel hoops were used as transverse tie reinforcement, with two spacings of 55 and 170 mm as shown in Fig. 1(a), and with an (f_y) of 220 MPa.

To further validate the model's predictions, particularly its capability of replicating cross-sections other than square, the model was used to simulate the axial behavior of three short cylindrical concrete columns confined by FRCM jackets, tested by Trapko [25]. The cylinders had a diameter of 113 mm, a height of 300 mm, and were confined by 1 to 3 layers of PBO-FCRM system. The specimens were tested under concentric load. Table 2 list the properties of the tested specimens.

3. Finite element modeling

3.1. Model description

The numerical models for the columns in [18,19] were developed using the commercial finite element software ANSYS APDL 17.2 [26]. Due to the un-symmetric eccentric loads present in some specimens and to provide a uniform modeling procedure, a full-size column model was constructed for all specimens. Fig. 1(c) shows various parts of the FE model. A mesh sensitivity analysis was conducted, which showed that an element side of 25 mm for the concrete core and other parts, is a suitable balance between accuracy and solution complexity (running time, desk space). The boundary conditions consisted of hinged-hinged ends with a single symmetry, as can be seen in Fig. 1.

In order to simulate the post-peak response, a displacement-loading method was used by applying an imposed axial displacement at the respective load point. Appropriate element types were used for the different parts of the strengthened column, and interfaces between dissimilar materials. Both material and geometric nonlinearities were considered, providing an accurate simulation of possible failure modes such as crushing and cracking in concrete and cementitious mortar, column buckling, and rupture of strengthening fibers. The following subsections discuss the modeling procedure undertaken in this analysis.

3.2. Element types

The concrete core is the main part of the column and it was modeled by an eight-node brick element SOLID185. This element has three translational degrees of freedom (DOF) per node, and can be used to represent various nonlinear properties such as plasticity, stress stiffening, large deformations, and large strains [26]. SOLID185 element was also used to model the steel plates present at column ends and the steel straps that were used in the experimental campaign to prevent end failure, see Fig. 1(c). The steel reinforcement (both longitudinal bars and ties) was modeled with the truss element (LINK 180), having two nodes and three translational DOF for each node. This element carries only axial stiffness and is capable of plasticity, large deflections and large strains [26].

The FRCM jacket was modeled by the four-node shell element (SHELL181), having six DOFs per node, three of which are translational and the remaining three are rotational. The element has both membrane and bending stiffnesses and is capable of large rotation, and/or large strain, and nonlinear analysis [26]. One of the element's main features is the multilayer definition, which is suitable for representing composite shells or sandwich construction [26]. When defining multilayered shell, the number of layers, layer thickness, layer orientation (relative to the element's local axis), layer material, and number of integration points per layer, are inputted.

The FRCM strengthening jacket is treated in this analysis as multilayered shell, consisting of several layers, which were (a) the internal mortar coating, (b) horizontal fiber mesh, (c) vertical fiber mesh, and (d) external mortar coating. In case more than one FRCM wrap is used, such as columns (C_2H, C_1V_1H, and C_1V_2H), the multilayer inputs

Table 1
Description of modeled columns and key FE results.

Specimen code.	FRCM layout		Eccentricity e, (mm)	Maximum load, P_{max} (kN)		% Diff.[1]	$P_{y\text{-}FEM}$[2] (kN)	% Difference[3]
	Horizontal	Vertical		Exp. ($P_{max\text{-}Exp}$)	FEM ($P_{max\text{-}FEM}$)			
C_0	—	—	0	2213.8	2247.4	1.52	2122.8	5.54
C_16	—	—	16	1652.0	1648.3	0.22	1611.3	2.24
C_32	—	—	32	1516.4	1331.0	12.23	1277.7	4.00
C_1H_0	1 layer	—	0	2586.8	2469.8	4.52	2188.1	11.40
C_1H_16	1 layer	—	16	1956.8	1810.3	7.49	1653.8	8.64
C_1H_32	1 layer	—	32	1596.0	1460.4	8.49	1300.7	10.93
C_2H_16	2 layers	—	16	2043.7	1855.5	9.21	1683.5	9.30
C_1V_1H_0	1 layer	1 layer	0	2227.0	2557.4	14.83	2237.6	12.50
C_1V_1H_16	1 layer	1 layer	16	1774.8	1940.7	9.34	1726.3	11.04
C_1V_1H_32	1 layer	1 layer	32	1612.5	1578.7	2.10	1432.3	9.27
C_1V_2H_32	2 layers	1 layer	32	1618.1	1629.1	0.68	1461.5	10.28

[1] $= \frac{P_{max-FEM} - P_{max-Exp.}}{P_{max-Exp.}} \times 100$.
[2] Load at first yielding of longitudinal steel reinforcement.
[3] $= \frac{P_{y-FEM} - P_{max-FEM}}{P_{max-FEM}} \times 100$, [where $P_{y\text{-}FEM}$ is the load at yielding of longitudinal steel from FE model].

Table 2
Properties of FRCM-confined cylinders and key experimental and FE results.

Specimencode.	Number of FRCM layers	t_f (mm)	f_{co} MPa)	f_{cc} (MPa)		Exp./FE	ε_{cc}		Exp./FE
				Exp.	FE		Exp.	FE	
M1-1	1	0.0455	22.60	32.66	33.39	0.98	0.0070	0.0068	1.03
M2-1	2	0.0455	22.60	42.48	44.50	0.95	0.0121	0.0131	0.92
M3-1	3	0.0455	22.60	55.80	57.78	0.97	0.0171	0.0211	0.81

t_f = equivalent fiber thickness in one FRCM layer; f_{co} = compressive strength of unconfined concrete; f_{cc} = peak compressive strength of confined concrete; ε_{cc} = peak axial strain of confined concrete.

Table 3
Shell element multi-layered definition for column C_1V_1H.

Layer No.	Type	Thickness, mm	Orientation[3]
1	Mortar	2.5[1]	0
2	Vertical PBO mesh	0.011[2]	90
3	Horizontal PBO mesh	0.046[2]	0
4	Mortar	2.5[1]	0
5	Mortar	2.5[1]	
6	Horizontal PBO mesh	0.046[2]	0
7	Vertical PBO mesh	0.011[2]	90
8	Mortar	2.5[1]	0

[1] Assumed value.
[2] Equivalent thickness of continuous layer, obtained by distributing fibers in PBO mesh evenly across the width.
[3] Relative to *x*-axis in Fig. 1(c).

(e.g. number of layers, orientation, and thickness) are modified based on the desired strengthening layout. Table 3, shows the multilayer definition for columns in group C_1V_1H. It should be noted that the shell element doesn't account for interlaminar slippage and delamination [26], assuming the mortar and fiber mesh are perfectly bonded.

The interface between the column and FRCM system is modeled by the contact element CONTA173, which has four nodes with three translational DOFs per node. The element was overlaid on the surface of FRCM system, while a target element (TARGE170) was glued to the column's surface, and interacted with the contact element via the contact-target set. The interfacial behavior at the concrete-mortar interface was assumed to be fully bonded, and was defined by a Multi-Point Constraint (MPC) contact algorithm. Interfacial slippage and debonding of FRCM system from concrete has been amply reported in literature for flexural and shear applications [6–8]. However, for column confinement application, which is not a bond critical problem [27], the interface condition doesn't significantly affect the column's axial behavior and is typically modeled as perfect bond [28–30].

3.3. Material properties

Concrete columns, whether confined or not, are typically idealized with a Drucker-Prager plasticity model [31,32], which takes into account concrete dilation under axial compression. Conventional DP models assume an elastic-perfectly plastic response under both tensile and compressive stresses, and utilize a modified version of the Von Mises yield criterion to account for the effects of hydrostatic pressure [31]. However, this model is unable to simulate the large difference in tensile and compressive responses of concrete and doesn't include softening after cracking or crushing [26].

In this study, the Drucker-Prager (DP) concrete model, available in recent ANSYS versions such as V17.2, was used to model the concrete core and cementitious mortar. DP-concrete is an improved version of the traditional DP model, adding several enhancements such as separate failure criteria for tension and compression, nonlinear stress-strain response in compression, stress softening/hardening in tension and compression, and post-cracking stress stiffening in tension [26]. Several hardening/softening behaviors for tension and compression, including linear, exponential, piece-wise linear, and fracture energy, are available with the model. The DP-concrete model is not available in the typical graphical user interface (GUI) of ANSYS but was implemented using a command subroutine.

The theoretical stress-strain relations of Kent and Park [33] and Lam and Teng [34] were implemented within the framework of DP-concrete to simulate the response of steel hoop-confined concrete (control columns) and FRCM-confined (strengthened columns), respectively. A detailed description of the theoretical stress-strain models can be found in the original articles in [14,15] or elsewhere in literature [4,27,31,35]. It should be noted that, for strengthened columns, only the confinement from external FRCM jacket is considered, while the coupling effects from the internal steel hoops where neglected. These effects are typically neglected in theoretical studies, but can be included in future investigations.

Table 4
Material properties used in modeling FRCM-confined RC columns.

Material	Elastic modulus (GPa)	Compressive strength (MPa)	Tensile strength (MPa)	Yield strength (MPa)	Poisson's ratio
Concrete	33[1]	49[2]	4.4[7]	—	0.2[8]
Cementitios mortar	6[2]	29[2]	3.5[2]	—	0.2[8]
Longitudinal steel reinforcement	200[3]	500[4]	500[4]	500[2]	0.3[8]
Steel stirrups	200[3]	500[4]	220[4]	220[2]	0.3[8]
Structural steel	200[3]	Note[5]	Note[5]	Note[5]	0.3[8]
PBO mesh	270[2]	3480[6]	5800[2]	—	0.35[8]

[1] Determined as $E = 4700\sqrt{f_c'}$ following ACI 318–14 code [36].
[2] From Trapko [18,19].
[3] Assumed, following Jawdhari and Harik [37].
[4] Equal to the yield strength, assuming an elastic-perfectly plastic response.
[5] Structural steel was assumed as linear elastic with no failure.
[6] Determined as 0.6 times the tensile strength, following Khan et al. [38].
[7] Determined as $f_t = 0.625\sqrt{f_c'}$ following ACI 318-14 code [36].
[8] Following [5,37].

Table 4 lists the material properties for concrete, cementitious mortar, longitudinal and shear steel reinforcements, and structural steel used for support plates and straps. Most properties were taken from tests by Trapko [18,19], but in case experimental values are not available, appropriate assumptions were made and referenced in Table 3. The steel longitudinal and shear reinforcements were modeled as elastic-perfectly plastic material, with yield strengths given in Table 4. The PBO mesh was modeled as linear elastic material up to failure. Material failure, including tensile rupture and compressive kinking, for the PBO mesh was simulated explicitly by the composite damage model (CDM) available in ANSYS along with a failure criteria based on maximum stress. In CDM, FRP failure initiates when the actual stresses reach the predefined maximum strength limits given in Table 4. After damage initiation, the material stiffness degrades according to an assumed stiffness reduction coefficient, which is taken as 0.95 in this study. Fig. 2 plots the material stress-strain relations for different parts of the column.

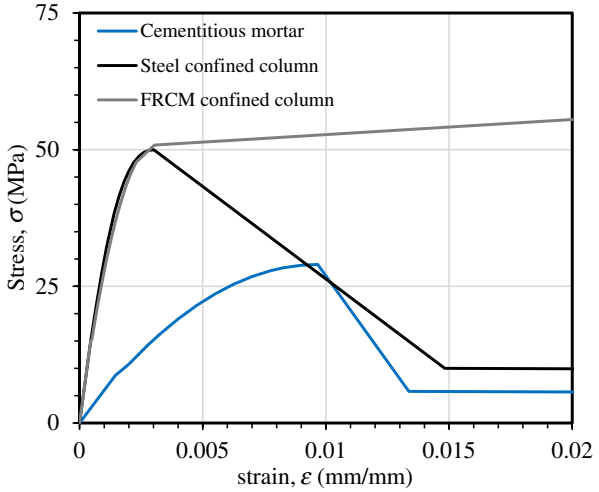

(a) Mortar and concrete

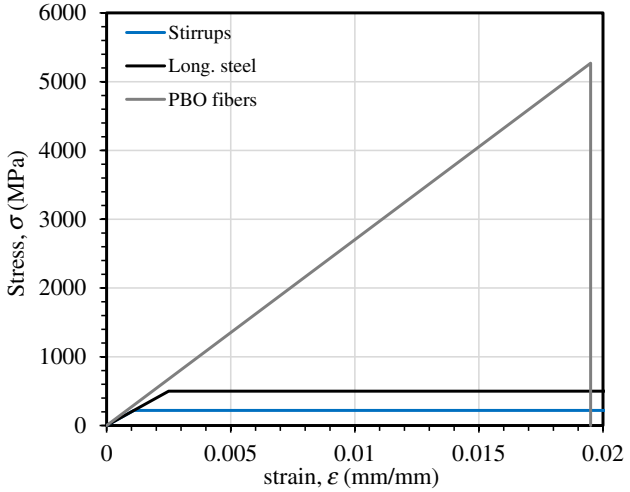

(b) Steel and PBO fibers

Fig. 2. Constitutive material models used in the FEM analysis.

4. Model validation

The model described in the previous section is used to simulate the eccentrically loaded RC columns confined with FRCM technique, tested by Trapko [18,19]. Table 1 describes the geometry and confinement layout of tested columns, and summarizes the key results from the FE models and experimental tests. The main comparison in this table is the ultimate load of RC columns. It can be noticed from this table that the ultimate load values obtained from FE models are predicted well with the maximum divergence being less than 15%, when compared to experimental values. The maximum difference between experimental and numerical values for the maximum load (P_{max}) was in specimen C-1V-1H-0. This divergence seems to be related to experimental issues, evident by the observation that the maximum load for this specimen, which is confined by two FRCM layers (one horizontal and one vertical) is less than that of the specimen confined by one layer only (specimen C-1H-0), and almost equal to the maximum load of the control specimen (C-0). In addition, the comparison between experimental and FE load-lateral deflection (P-Δ) curves for selected columns is presented in Fig. 3. The model P-Δ behavior was mostly softer than the experimental curves, but within acceptable ranges.

To increase the reliability of the FE results, the readings of longitudinal strain gages attached to FRCM surface and positioned in mid-height of the columns, on the side experiencing compression, were compared with the corresponding FE values as shown in Fig. 4. The load-longitudinal strain curves obtained from FE model are generally softer but within acceptable ranges, as compared to the experimental results. In addition, Fig. 5 presents the experimental and FE predicted load vs. transverse strain plots for three representative samples with load eccentricities of 16 and 32 mm, obtained from two transverse strain gages, one from the tension side (H7 in Fig. 5) and the other from the compression side (H2 in Fig. 5). The comparison between the experimental readings and FE predictions showed a high level of accuracy for the predicted trend with reasonable agreement along the load

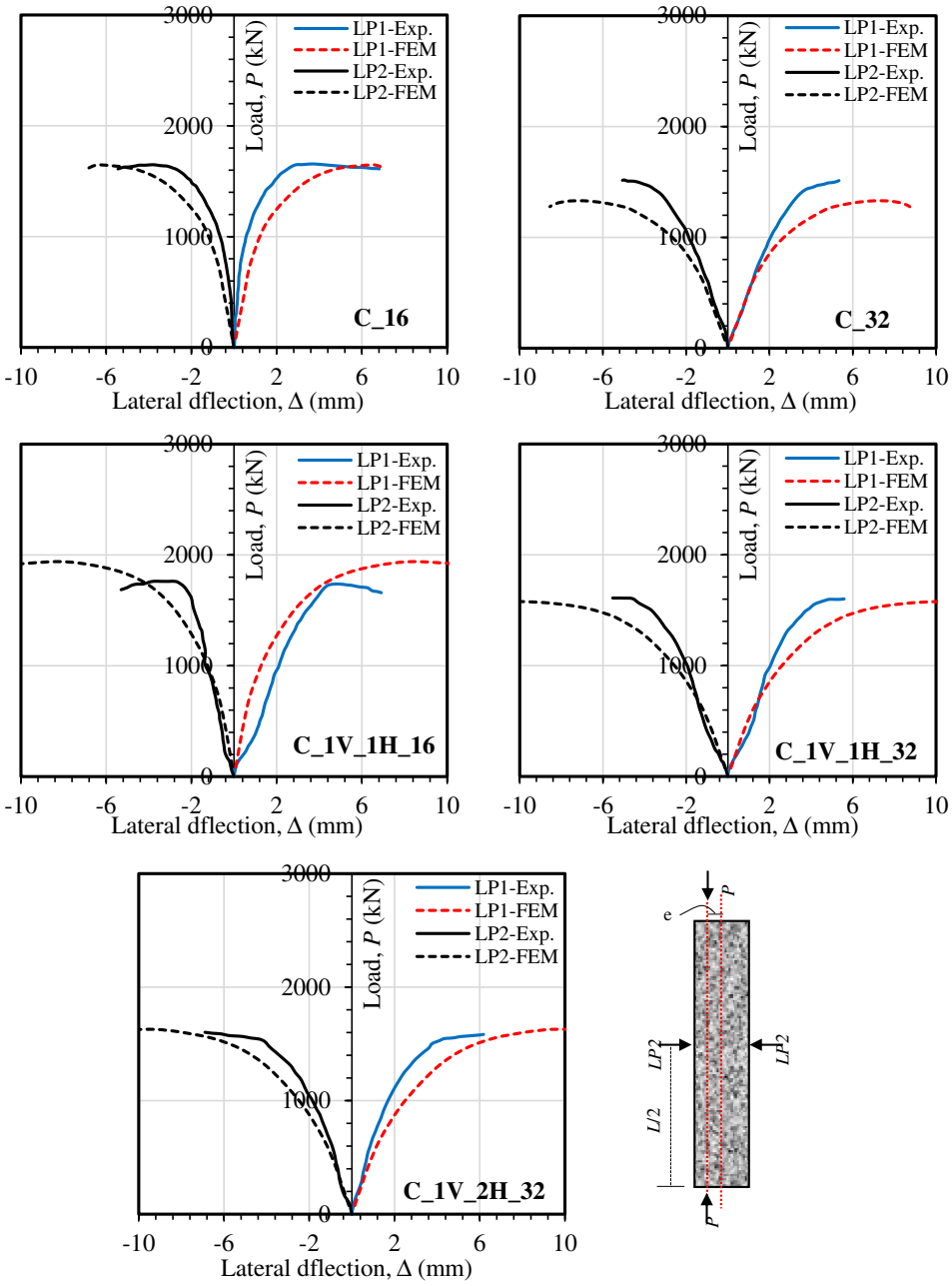

Fig. 3. Load vs. lateral deflection (P-Δ) curves, from FE models and tests.

application. The model's slight divergence from test results for lateral deformations and strains can be related to the concrete dilation and Poisson's ratio effects, which are difficult to simulate in most finite element programs.

In addition, prediction of failure modes, can provide another means of validating the FE model. One of the failures observed experimentally was fracture of the cementitious mortar, Fig. 6. The FE model was able to simulate this failure as can be noticed from the large values of plastic strains in Fig. 6 for two selected columns, with shown strains exceeding the mortar's fracture strain in Fig. 2(a) and indicating mortar's fracture.

Due to presence of the FRCM jacket, it was not experimentally possible to observe the governing failure mode inside the concrete core, and authors of the experimental study reported only the physical failure of the FRCM jacket seen in Fig. 6. Thus, the FE model could be used to analyze the confined specimens and confirm the governing failure mode. Fig. 7 plots the plastic strains at ultimate load for several confined specimens, as obtained from the FE model. It can be seen that specimens with concentric loads (e.g. C_1H_0) failed by concrete crushing at multiple locations along the column's height and faces. For columns with eccentricity e = 16 mm, crushing failure occurred in the face experiencing compression, while no cracking was observed in the opposite tensioned face. However, when e increased to 32 mm, cracks appeared in the tensioned face, in addition to crushing of the compressed face, Fig. 7. The FE model also showed a yielding of the longitudinal steel reinforcement in all specimens. After the yielding loads, specimens were only able to carry negligible additional loads, 5% for control specimens and 11% for confined specimens, as can be seen in Table 1.

The concrete cylinders in Trapko [25] were modeled following the same modeling procedure discussed in Section 4 for the long, square RC columns. SOLID185 and SHELL181 elements were used to model the concrete cylinder and FRCM jacket, respectively. The element side length was maintained at 10 mm. The bottom face of the concrete core was fixed in all three translational directions. The top face was restrained in the two transverse directions and was given a displacement-

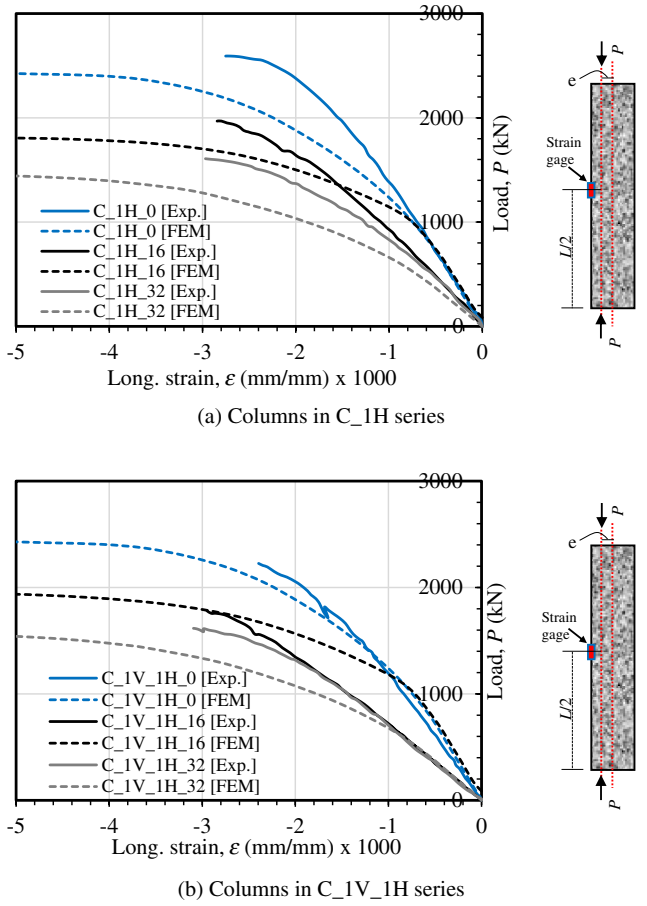

(a) Columns in C_1H series

(b) Columns in C_1V_1H series

Fig. 4. Load vs. longitudinal strain (P-ε) curves, from FE models and tests.

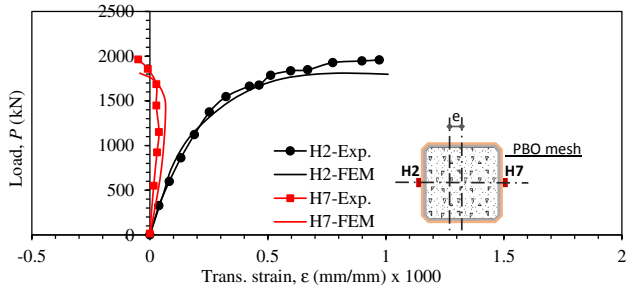

(a) Column in C_1H_16

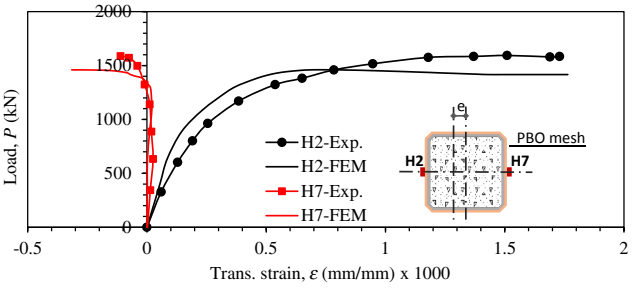

(b) Column in C_1H_32

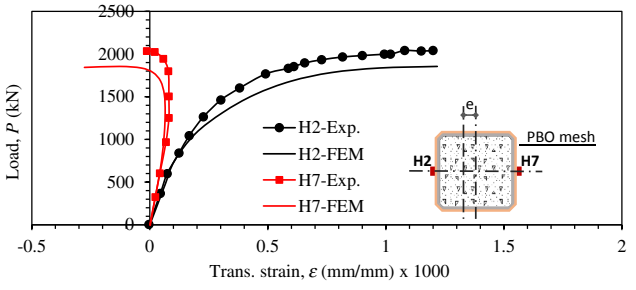

(c) Column in C_2H_16

Fig. 5. Load vs. transverse strain (P-ε) curves, from FE models and tests.

controlled load in the vertical direction. Table 2. List the key experimental and finite element results, including the peak compressive strength of confined concrete (f_{cc}) and corresponding peak strain values (ε_{cc}). It can be noticed from this table that the values of peak strength are strongly affected by the number of PBO mesh layers. This trend is exactly the same for both experimental and FE results. With regard to the accuracy of FE model in predicting the value of peak strength, the maximum divergence between experimental and FE results was less than 5%. However, this value was around 19% when the peak strain was compared. In both cases, the FE model seems be able to predict the experimental results with reasonable agreement.

Fig. 8 shows the stress-strain curves of the three specimens tested by Trapko [25] with the corresponding FE results. The shape of the stress-strain curves is similar for all specimens for both experimental and FE results, showing a generally bilinear hardening trend. As can be seen in the figures, the slope of the second line (E_2) increases proportionally with the number of applied FRCM layers. This trend is observed in the both experimental and FE results which reflects the ability of the FE model to predict the behavior of concrete jacketed with FRCM system with a high degree of accuracy. The results also show the ability of FE model in simulating different cross-section shapes.

5. Parametric study

The validated model was used in a comprehensive parametric study, comprising 96 new models, to examine the effects of key variables expected to impact the behavior of FRCM-confined RC columns. These parameters were the column cross-sectional shape; and for rectangular columns, the aspect ratio (h/b); slenderness ratio (KL/r); eccentricity (e) with emphasis on (e) outside of the column section; and concrete compressive strength ($\acute{f}_c$). For each parameter, both un-strengthened and FRCM-confined models were constructed, to evaluate the contribution of FRCM technique on the examined variable. One layer of horizontal FRCM jacket was utilized in all models comprising the parametric analysis. The following sub-sections describe the studies parameters and their observed effects.

5.1. Column's cross-section shape

Due to lack of experimental data on cross-sectional shapes other than square tested by Trapko [18,19], the finite element model can be used to preliminarily examine the effects of this important parameter. The Drucker-Prager constitutive material model featured in the FE model for simulating confinement in concrete columns has been amply and successfully used in finite element studies of FRP-confined concrete columns with different cross-sections [28,30–31]. Four commonly used column cross-sections were investigated, namely square, circle, hexagon, and octagon. The area for each shape was kept constant and equal to that of the square cross-section used in experimental study of Trapko [18,19]. The column's length, material properties, reinforcement ratio, FRCM details, boundary conditions and other properties were un-changed. ACI 318-14 [36] code recommendations were followed to detail the longitudinal reinforcement in the new cross-sections. Fig. 9(a) shows the FE models for columns having the four examined cross-sections. Concentric load ($e = 0$), and two eccentric loads, at $e = 16$ and $e = 32$ mm, were considered, for each shape.

Based on ultimate loads for FRCM-confined columns [Table 5, Fig. 9(c)], circular section seems to give the highest P_{max} for all

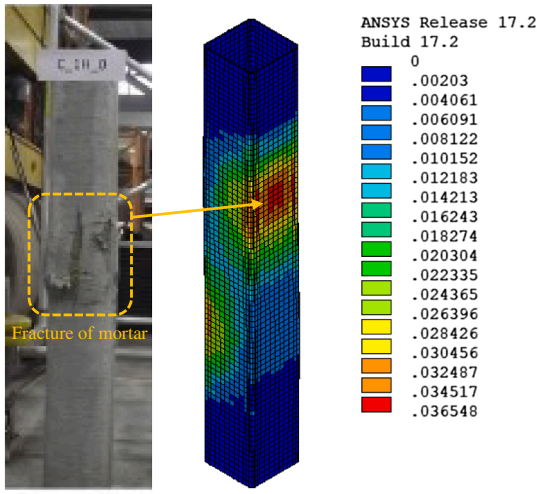

(a) Column: C_1H_0

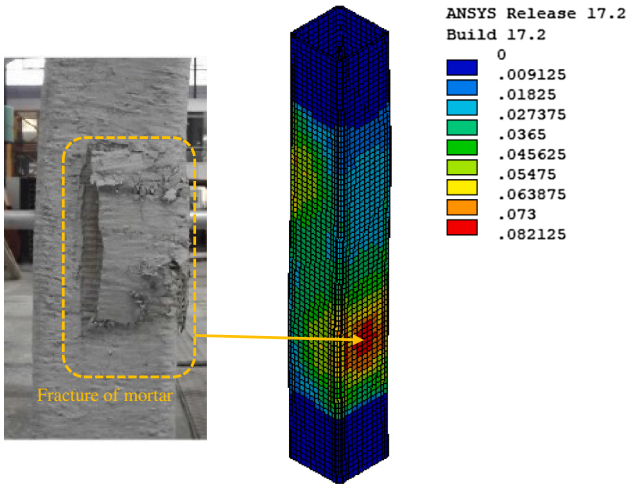

(b) Column: C_1H_16

Fig. 6. FE predictions of fracture in cementitious mortar, showing plastic strain index.

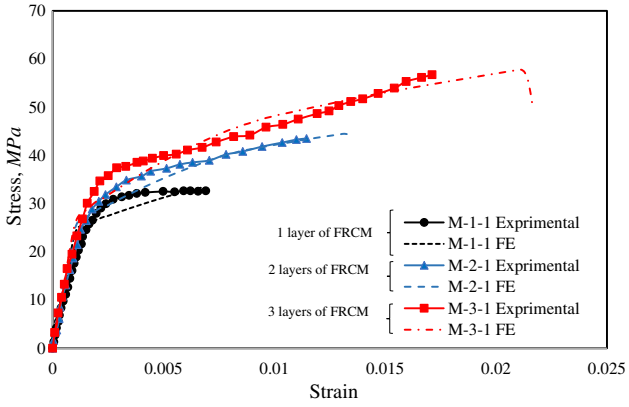

Fig. 8. Comparison between stress-strain curves of confined concrete cylinders obtained from experimental [25] and FE results.

eccentricities, with square and octagon having comparable P_{max}., and hexagon having the least. For un-confined columns, all sections resulted in a comparable P_{max}., with ultimate load varying randomly with eccentricity, Fig. 9(c). The FRCM contribution, determined according to Table 4, was in average 9.8% for the square, 15.6% for the circle, 6.9% for the hexagon, and 8.5% for the octagon. The failure mode for all sections was by concrete crushing proceeded by yielding of tensile steel, as confirmed by the high values of longitudinal strains (ε_y) in Table 5 and post-processing analysis of steel stresses. The longitudinal and hoop strains, and other results are shown in Table 5.

Fig. 9(b) plots the load (P) versus mid-height lateral deflection (Δ) curve for all FRCM-confined columns, at $e = 16$ mm. At the elastic range, all shapes had a similar initial stiffness. After $P = 1000$ kN, the octagon showed a softer pre-peak stiffness than other shapes but a stiffer post-peak response, probably due to geometrical un-symmetry relative to the line of load. Fig. 9(c) plots maximum load (P_{max}) versus cross-sectional shape, showing the effects of eccentricity for un-confined and FRCM-confined columns. All shapes showed a decrease in P_{max}, ranging from 39 to 45%, as the eccentricity increased from 0 to 32 mm.

5.2. Aspect ratio of rectangular column

The aspect (h/b) ratio, where h is the side parallel to the load

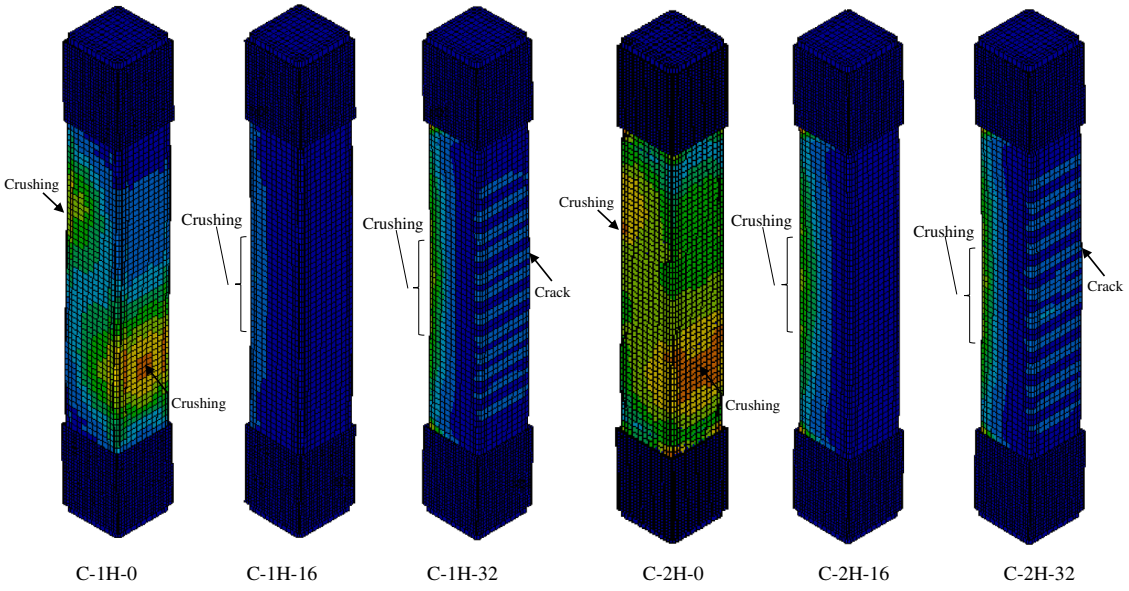

Fig. 7. Plastic strain indices at ultimate load in several columns, showing cracking and crushing failures.

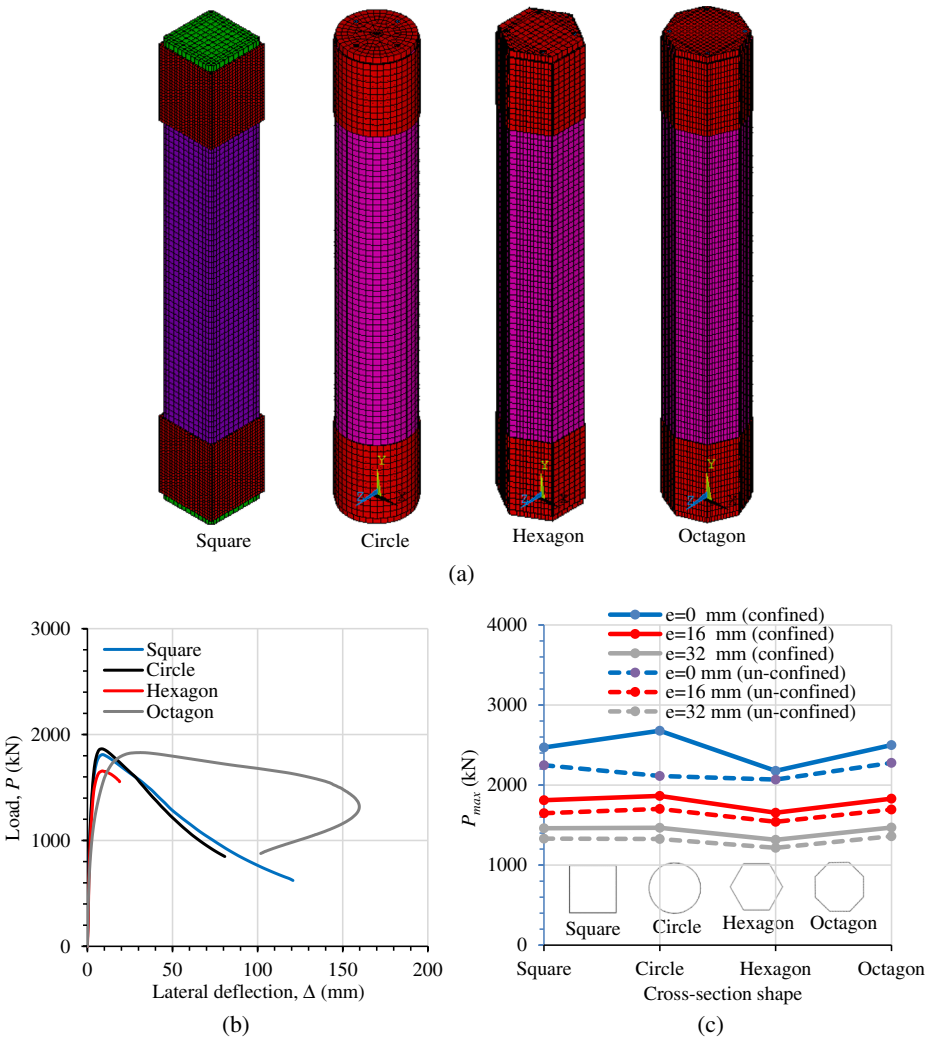

Fig. 9. Effects of column cross-sectional shape, (a) generated FE models, (b) load vs. mid-height lateral deflection curve for e = 16 mm, (c) maximum load (P_{max}) vs. cross- sectional shape.

Table 5
Results of parametric study on column cross-section shape.

Column shape	Eccentricity, e (mm)	Un-strengthened			Strengthened			FRCM contribution[3]	Type of failure[4]
		P_{max} (kN)	ε_x[1]	ε_y[2]	P_{max} (kN)	ε_x[1]	ε_y[2]		
	0	2247	0.0018	−0.0038	2470	0.0065	−0.0112	9.90	SY, CC
	16	1648	0.0026	−0.0048	1810	0.0035	−0.0069	9.82	SY, CC
	32	1331	0.0023	−0.0043	1460	0.0031	−0.0064	9.72	SY, CC
	0	2113	0.0061	−0.0118	2679	0.0178	−0.0226	26.79	SY, CC
	16	1702	0.0039	−0.0065	1864	0.0049	−0.0076	9.52	SY, CC
	32	1326	0.0054	−0.0085	1466	0.0052	−0.0079	10.56	SY, CC
	0	2068	0.0018	−0.0035	2177	0.0023	−0.0044	5.27	SY, CC
	16	1541	0.0016	−0.0038	1655	0.0035	−0.0061	7.40	SY, CC
	32	1216	0.0152	−0.0220	1316	0.0040	−0.0067	8.22	SY, CC
	0	2277	0.0019	−0.0039	2499	0.0078	−0.0133	9.74	SY, CC
	16	1695	0.0031	−0.0057	1830	0.0052	−0.0096	7.96	SY, CC
	32	1361	0.0024	−0.0042	1470	0.0040	−0.0072	8.00	SY, CC

[1] ε_x = hoop strain at maximum load (P_{max}).
[2] ε_y = longitudinal strain at maximum load (P_{max}).
[3] FRCM contribution= $\frac{P_{max}(strengthened) - P_{max}(un-strengthened)}{P_{max}(un-strengthened)} \times 100$
[4] Type of failure: CC = concrete crushing, SY = steel yield, B = buckling.

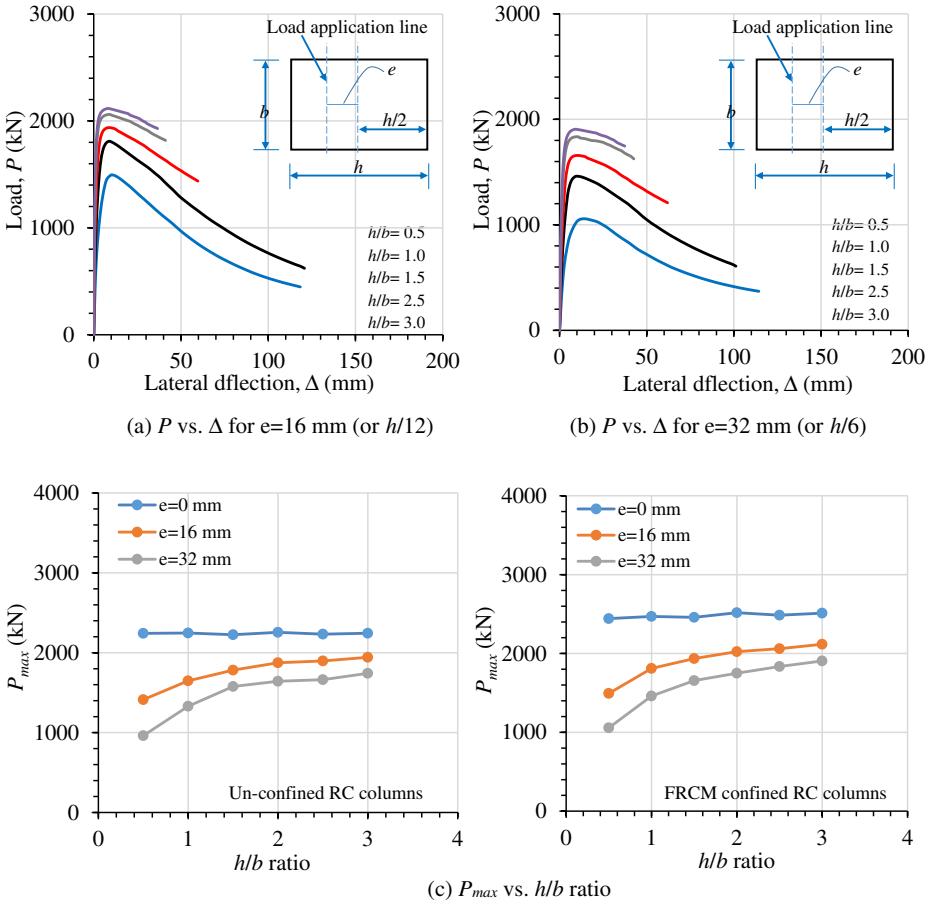

Fig. 10. Effects of h/b ratio on FRCM-strengthened RC columns.

eccentricity and b is the one perpendicular to, as shown in Fig. 10, is examined by varying (h/b) ratio from 0.5 to 3, at 0.5 increment. The total cross-sectional area was constant for all (h/b) ratios and equals to the original value in experimental study of Trapko [18]. The column's length, material properties, reinforcement ratio, FRCM details, boundary conditions and other properties were un-changed. Three eccentricity values, e = 0, 16, 32 mm, were considered for each (h/b) ratio.

Fig. 10(a and b) shows the P-Δ curves in FRCM-confined columns for different (h/b) ratios, at e = 16 and e = 32 mm, respectively. Fig. 10(c) plots the P_{max} versus (h/b) ratio curves for both un-strengthened columns and FRCM-confined ones, at e = 0, 16, 32 mm. Fig. 10 shows that, for concentric load (e = 0 mm) and for both un-strengthened and FRCM-confined columns, P_{max} is not affected by (h/b) ratio. However, for eccentric loads, P_{max} is seen to increase with (h/b) ratio, sharply at h/b = 0.5 to 1.5, and then insignificantly at h/b = 1.5–3.0. For example, P_{max} of FRCM-confined columns increased by 30 and 57%, for e = 16 and 32 mm, respectively, when h/b increased from 0.5 to 1.5. However, the increase in P_{max} was only 9 and 15% when h/b increased from 1.5 to 3, for the same respective eccentricities. Similar trend was also observed in control columns, as seen in Fig. 10(c). The P-Δ curves of both eccentric loads show a stiffer pre-peak response and tendency to fail at lower lateral deflection, when h/b increases, as can be seen in Fig. 10(a and b).

Table 6 gives a numerical list of key results, based on the effects of (h/b) ratio. The FRCM contribution, determined from P_{max} of control and confined columns, was in average 9.1%, showing no clear variation with (h/b) ratio or eccentricity. Observed failure mode for all h/b and eccentricity values was by concrete crushing proceeded by yielding of tensile steel, as confirmed by the large values of longitudinal strains (ε_y) and post-processing analysis of steel stresses.

The ductility of the analyzed specimens was also quantified by calculating the "energy index" which represents the area under the stress-strain curve up to ultimate load [17] as listed in Table 6. It is evident from this table that the ductility energy indices increase for the strengthened specimens tested under the same loading condition. This improvement in ductility was also found in previous studies such as [17,18]. In addition, the ductility indices increase when h/b ratio is increased for the strengthened specimens, because of increasing the section perimeter and hence FRCM jacket area, for the same cross-section area. However and for the un-strengthened specimens, h/b ratio has no clear influence on the ductility index.

5.3. Slenderness ratio

The column's slenderness can be expressed as ratio (KL/r), where K is a factor used to convert the actual column length to an effective buckling length depending on the end conditions; L is the column's length between supports; r is the radius of gyration of the column's cross-section calculated as $r = \sqrt{I/A}$ where I is the moment of inertia and A is the cross-sectional area. For the hinged-hinged columns modeled in this study, K is equal to 1.0. Four values for (KL/r) ratio, namely: 10, 25, 50, and 75, were examined in this study covering different conditions from stubby to slender, by varying the column's length while keeping cross-section unchanged and equal to that in the experimental tests.

Fig. 11(a and b) shows the P-Δ curves in FRCM-confined columns for different (KL/r) ratios, at e = 16 and e = 32 mm, respectively. Fig. 11(c) plots the P_{max} versus (KL/r) ratio curves for both un-strengthened columns and FRCM-confined ones, at e = 0, 16, 32 mm. For concentric load, P_{max} doesn't appear to be affected by (KL/r) ratio for both un-strengthened and FRCM-confined columns, as shown in

Table 6
Results of parametric study on column's aspect (h/b) ratio.

h/b ratio	Eccentricity, e (mm)	Un-strengthened				Strengthened				FRCM contribution[4]	Type of failure[5]
		P_{max} (kN)	ε_x[1]	ε_y[2]	E_i[3] (MPa)	P_{max} (kN)	ε_x[1]	ε_y[2]	E_i[3] (MPa)		
0.5	0	2243	0.0018	−0.0037	0.151	2442	0.0066	−0.0106	0.559	8.87	SY, CC
	16	1413	0.0022	−0.0042	0.110	1493	0.0027	−0.0048	0.133	5.66	SY, CC
	32	963	0.0021	−0.0041	0.076	1057	0.0034	−0.0052	0.106	9.76	SY, CC
1	0	2247	0.0018	−0.0038	0.153	2470	0.0065	−0.0112	0.607	9.90	SY, CC
	16	1648	0.0026	−0.0048	0.151	1810	0.0035	−0.0069	0.355	9.82	SY, CC
	32	1331	0.0023	−0.0043	0.106	1460	0.0031	−0.0064	0.179	9.72	SY, CC
1.5	0	2225	0.0017	−0.0036	0.144	2459	0.0122	−0.0184	1.043	10.52	SY, CC
	16	1782	0.0024	−0.0045	0.143	1936	0.0056	−0.0092	0.553	8.86	SY, CC
	32	1578	0.0022	−0.0042	0.126	1657	0.0055	−0.0091	0.309	5.00	SY, CC
2	0	2255	0.0018	−0.0037	0.148	2518	0.0145	−0.0217	1.315	11.66	SY, CC
	16	1874	0.0029	−0.0052	0.128	2024	0.0064	−0.0103	0.505	8.00	SY, CC
	32	1643	0.0031	−0.0055	0.121	1775	0.0064	−0.0104	0.359	8.03	SY, CC
2.5	0	2233	0.0018	−0.0036	0.142	2486	0.0145	−0.0211	1.207	11.33	SY, CC
	16	1897	0.0025	−0.0044	0.128	2061	0.0074	−0.0114	0.514	8.64	SY, CC
	32	1663	0.0023	−0.0043	0.126	1835	0.0069	−0.0110	0.427	10.34	SY, CC
3	0	2244	0.0016	−0.0035	0.151	2511	0.0155	−0.0224	1.266	11.90	SY, CC
	16	1943	0.0029	−0.0052	0.135	2117	0.0075	−0.0117	0.536	8.95	SY, CC
	32	1742	0.0032	−0.0056	0.127	1906	0.0066	−0.0104	0.476	9.41	SY, CC

[1] ε_x = hoop strain at maximum load (P_{max}).
[2] ε_y = longitudinal strain at maximum load (P_{max}).
[3] E_i = ductility energy index.
[4] FRCM contribution= $\frac{P_{max}(strengthened) - P_{max}(un-strengthened)}{P_{max}(un-strengthened)} \times 100$
[5] Type of failure: CC = concrete crushing, SY = steel yield, B = buckling.

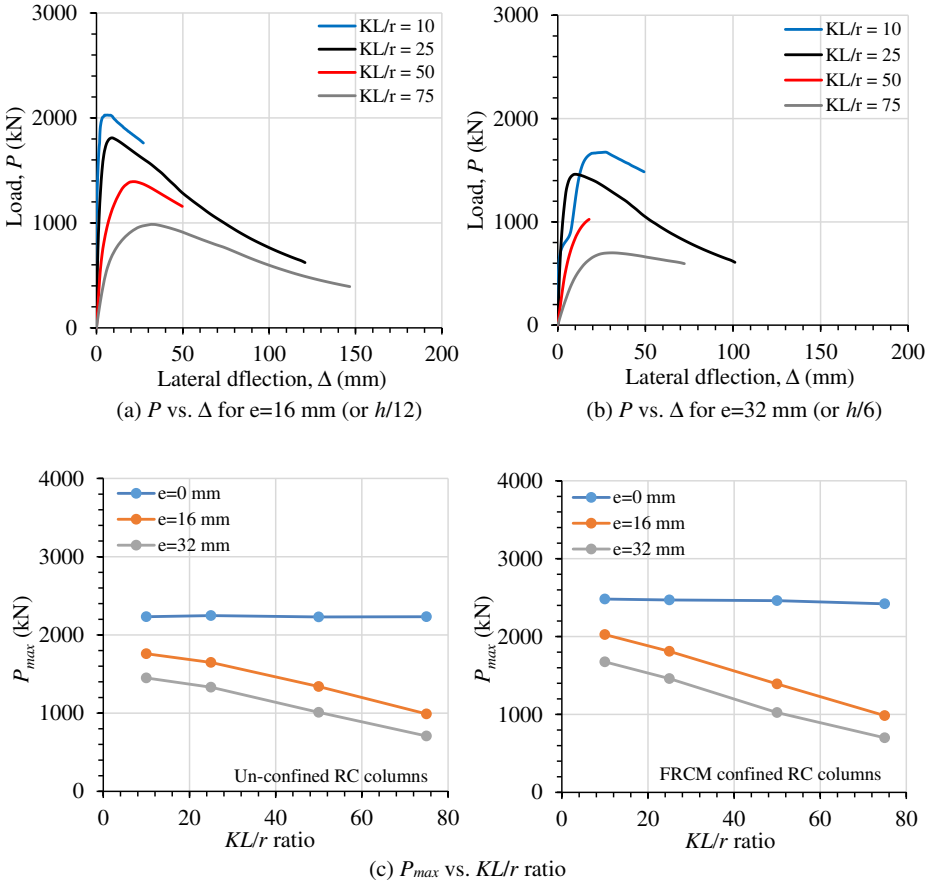

Fig. 11. Effects of KL/r ratio on FRCM-strengthened RC columns.

Table 7
Results of parametric study on slenderness (KL/r) ratio.

KL/r ratio	Eccentricity, e (mm)	Un-strengthened				Strengthened				FRCM contribution[4]	Type of failure[5]
		P_{max} (kN)	ε_x[1]	ε_y[2]	E_i[3] (MPa)	P_{max} (kN)	ε_x[1]	ε_y[2]	E_i[3] (MPa)		
10	0	2233	0.0021	−0.0039	0.156	2481	0.0374	−0.0359	2.128	11.10	SY, CC
	16	1759	0.0029	−0.0053	0.164	2025	0.0163	−0.0254	1.188	15.12	SY, CC
	32	1450	0.0030	−0.0054	0.144	1675	0.0204	−0.0302	1.177	15.52	SY, CC
25	0	2247	0.0018	−0.0038	0.153	2470	0.0065	−0.0112	0.607	9.90	SY, CC
	16	1648	0.0026	−0.0048	0.151	1810	0.0035	−0.0069	0.355	9.82	SY, CC
	32	1331	0.0023	−0.0043	0.106	1460	0.0031	−0.0064	0.179	9.72	SY, CC
50	0	2230	0.0021	−0.0038	0.153	2461	0.0055	−0.0091	0.479	10.36	SY, CC
	16	1340	0.0017	−0.0035	0.085	1392	0.0019	−0.0039	0.100	3.88	SY, CC
	32	1010	0.0017	−0.0032	0.057	1024	0.0012	−0.0027	0.046	1.38	SY, CC
75	0	2232	0.0019	−0.0039	0.158	2420	0.0032	−0.0058	0.277	8.42	SY, CC
	16	989	0.0009	−0.0022	0.045	985	0.0011	−0.0024	0.043	0.00	B
	32	707	0.0006	−0.0017	0.019	700	0.0013	−0.0022	0.027	0.00	B

[1] ε_x = hoop strain at maximum load (P_{max}).
[2] ε_y = longitudinal strain at maximum load (P_{max}).
[3] E_i = ductility energy index.
[4] FRCM contribution= $\frac{P_{max}(strengthened) - P_{max}(un-strengthened)}{P_{max}(un-strengthened)} \times 100$.
[5] Type of failure: CC = concrete crushing, SY = steel yield, B = buckling.

Fig. 11(c). While for eccentric loads, P_{max} linearly decreases with the increase in (KL/r) ratio, as a result of second order moment effects. For FRCM-confined columns, P_{max} decreased by 52 and 58% when KL/r increased from 10 to 75, for e = 16 and 32 mm, respectively. The pre-peak stiffness of P-Δ curve of eccentrically-loaded columns (i.e. e = 16, 32 mm) decreases with the increase of KL/r, as can be seen in Fig. 11(a and b).

Table 7 gives a numerical list of key results, based on the effects of (KL/r) ratio. The FRCM contribution, determined from P_{max} of control and confined columns, is seen to be decreasing with the increase of (KL/r) ratio. The contribution is in average 13.9%, 9.8%, 5.2%, and 2.3% for (KL/r) ratio of 10, 25, 50, and 75, respectively. A material failure mode, controlled by yielding of longitudinal steel rebars and then crushing of concrete, was dominating in most KL/r ratios and eccentricities. However, at KL/r = 75 and e = 16, 32 mm, the failure mode shifted to stability by global buckling, Table 7. Based on the small values of FRCM contribution in Table 7, it can be assumed that a KL/r of 50 is the critical value differentiating between short and slender columns for the investigated FRCM-confined columns.

Regarding the ductility energy index, it can be seen in Table 7 that the FRCM strengthened columns have higher ductility indices than the corresponding un-strengthened columns which is similar to that discussed in the previous section. It also noticed from this table that the ductility indices increase as KL/r ratio decrease for the strengthened columns.

5.4. Eccentricity

Effects of load eccentricity (e) were investigated in this study by varying e as a ratio (e/h) of the side (h), from 0 to 2.5, corresponding to a maximum e of 500 mm. This parameter was identified in the experimental study of Trapko [18,19] to be extremely important, but their investigation was limited to e/h of 0.16 due to the difficulties associated with experimentally applying eccentricity outside the column's cross-section. Nevertheless, it is relatively easy to apply different e/h ratios in finite element analysis. The columns selected for investigating e/h effects in the un-confined and FRCM-confined configurations, were C_0 and C_1H_0, respectively, with the latter being confined by one layer of horizontal FRCM jacket, Table 1.

Fig. 12 plots the maximum load (P_{max}) versus e/h ratio for the un-confined and FRCM-confined RC columns, from either experimental tests or FE models. It can be seen that the FE models were able to predict P_{max} for the e/h range of 0–0.16 tested experimentally, for both control and confined columns. More importantly, the FE results show that P_{max} is decreasing almost linearly by 87% in average, when e/h ratio increased from 0 to 0.5, for control and confined columns. A slow decrease in P_{max} occurs when e/h increased from 0.5 to 2.5. The bilinear trend shown in Fig. 12 with the divider between the two lines being located at e/h of 0.5, might be attributed to a change of behavior from that of an axial member at $e/h \leq 0.5$ to that of a beam member, when e/h exceeds 0.5.

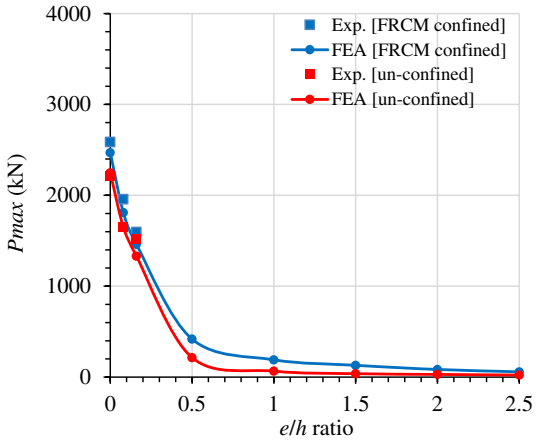

Fig. 12. Maximum load (P_{max}) vs. e/h ratio.

5.5. Concrete strength

The concrete's unconfined compressive strength (f'_c) of the column is one of the important parameters expected to affect the behavior of FRCM-confined concrete columns. This parameter was investigated in this study by utilizing three values for f'_c = 20, 35, and 50 MPa, for both the un-confined (control) and FRCM-confined cases, and for each of the eccentricity values, e = 0, 16, and 32 mm. The selected f'_c values were chosen to cover most ranges for the normal strength concrete class, assuming this class has more need for strengthening and confinement than high or ultra-high strength concrete.

Fig. 13(a) and (b) plot the P-Δ curves in FRCM-confined columns for the three f'_c values, at e = 16 and e = 32 mm, respectively. Fig. 13(c)

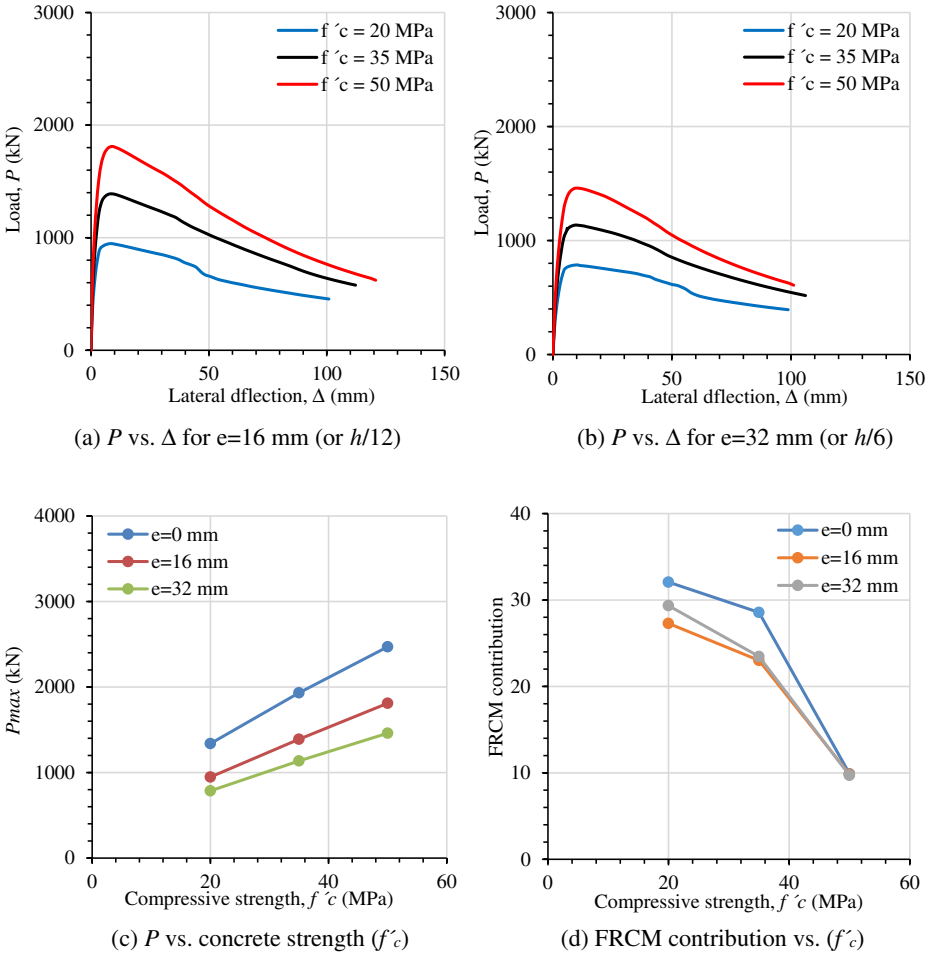

(a) P vs. Δ for e=16 mm (or h/12) (b) P vs. Δ for e=32 mm (or h/6)

(c) P vs. concrete strength (f'_c) (d) FRCM contribution vs. (f'_c)

Fig. 13. Effects of concrete strength (f'_c) on FRCM-strengthened RC columns.

plots the P_{max} versus f'_c curves for FRCM-confined ones, at e = 0, 16, 32 mm. For both the concentric and eccentric loadings, P_{max} increased linearly when f'_c increased from 20 to 50 MPa. In addition, the column's ductility, defined by the area under P-Δ curve, seems to also increase with increasing f'_c, as can be seen in Fig. 13(a), (b). The FRCM contribution, which is defined in Section 6.1 and in following sections as well as in Tables 5–7, is plotted in Fig. 13(d) in relation to f'_c, for the three examined eccentricities. The contribution was maximum, in average 29.5% for all eccentricities, at f'_c = 20 MPa. It then reduced slowly to 25% for f'_c = 35 MPa, and then sharply to 9.8%, for f'_c = 50 MPa. This results implies that FRCM confinement works best with low strength concrete, while minimum effects can be expected for high strength concrete.

6. Conclusions

In this study, a detailed three-dimensional finite element (FE) model was developed to study the behavior of RC columns confined by fiber-reinforced cementitious mortar (FRCM), under concentric and eccentric loads. The model utilized a new, improved version of the Druker Prager (DP) model specifically designed for concrete axial members, with a capability of including nonlinear compression, and softening/hardening in both tension and compression. The failure in fiber mesh and buckling in the column, were also considered, by using a composite damage model and activating geometrical nonlinearity, respectively. After validation with 11 full-scale column tests, featuring different number of FRCM layers and configurations, as well as different load eccentricities, the model was used in a comprehensive parametric study to investigate key parameters, namely: column' cross-sectional shape; aspect (h/b) ratio of rectangular columns; slenderness (KL/r) ratio; load eccentricity (e) as a ratio (e/h) to side (h); and concrete strength (f'_c). The following are conclusions drawn from result of this study:

1. The maximum load (P_{max}) obtained the FE model was within 15% divergence from experimental values. The FE model showed that the governing failure is concrete crushing preceded by yielding of internal steel reinforcement.
2. Circular cross-section yielded the highest P_{max} for FRCM-confined columns, followed by square and octagon, with hexagon being the least. The FRCM contribution was in average 9.8% for the square, 15.6% for the circle, 6.9% for the hexagon, and 8.5% for the octagon.
3. For concentrically loaded columns, P_{max} is not affected by the variation in column's aspect ratio (h/b). However, P_{max} is seen to increase sharply at h/b = 0.5–1.5, and then negligibly at h/b = 1.5–3.0, for eccentrically loaded columns.
4. P_{max} is unaffected by the column's slenderness ratio (KL/r), for concentrically loaded confined columns. For loads at eccentricity e = 16, 32 mm, P_{max} linearly decreases by 55% in average, when (KL/r) increases from 10 to 75. Also, the FRCM contribution is seen to decrease with the increase in (KL/r) ratio. A stability failure by buckling was seen at KL/r of 75, with KL/r = 50 estimated to be the threshold of stability failure, based on the negligible FRCM contribution at larger KL/r ratios.
5. P_{max} decreases almost linearly by 87% in average, when the eccentricity ratio (e/h) increased from 0 to 0.5, for control and confined columns. A slow decrease in P_{max} occurs when e/h increased from 0.5 to 2.5. This bilinear trend, with the divider being at $e/$

h = 0.5, might be attributed to change from axial to bending behavior.

6. Increasing $\acute{f}_c$ from 20 to 50 MPa resulted in a linear increase of P_{max} by 87% and improved ductility. However, FRCM contribution decreased from 29.5% to only 9.8% when $\acute{f}_c$ increased from 20 to 50 MPa.
7. The study showed that FRCM system can be used to confine concrete columns, resulting in an increase of strength ranging from 0 to 32%, depending on material and geometric parameters. The system is favorable over conventional FRP jacketing, due to using cementitious mortar as a binder instead of epoxy resin, which has a number of serviceability and safety concerns.

CRediT authorship contribution statement

Akram Jawdhari: Conceptualization, Methodology, Project administration, Resources, Software, Supervision, Validation, Writing - original draft, Writing. **Ali Hadi Adheem:** Conceptualization, Data curation, Formal analysis, Investigation, Software, Validation, Visualization, Writing - original draft. **Majid M.A. Kadhim:** Conceptualization, Methodology, Resources, Software, Supervision, Visualization, Writing - original draft, Writing - review & editing.

Declaration of Competing Interest

The authors declare that they have no known competing financial interests or personal relationships that could have appeared to influence the work reported in this paper.

Appendix A. Supplementary material

Supplementary data to this article can be found online at https://doi.org/10.1016/j.engstruct.2020.110504.

References

[1] Hashemi S, Al-Mahaidi R. Experimental and finite element analysis of flexural behavior of FRP-strengthened RC beams using cement-based adhesives. Constr Build Mater 2012;26(1):268–73.
[2] Jawdhari A, Peiris A, Harik I. Experimental study on RC beams strengthened with CFRP rod panels. Eng Struct 2018;173:693–705. https://doi.org/10.1016/j.engstruct.2018.06.105.
[3] El-Mogy M, El-Ragaby A, El-Salakawy E. Flexural behavior of continuous FRP-reinforced concrete beams. J Compos Constr 2010:669–80. https://doi.org/10.1061/(ASCE)CC.1943-5614.0000140.
[4] Florut SC, Sas G, Popescu C, Stoian V. Tests on reinforced concrete slabs with cutout openings strengthened with fibre-reinforced polymers. Compos Part B Eng 2014;66:484–93.
[5] Jawdhari A, Harik I. Finite element analysis of RC beams strengthened in flexure with CFRP rod panels. Constr Build Mater 2018;163:751–66. https://doi.org/10.1016/j.conbuildmat.2017.12.139.
[6] Wiberg A. Strengthening of concrete beams using cementitious carbon fibre composites Doctoral thesis Stockholm: Sweden: Royal Institute of Technology; 2003
[7] Ombres L. Flexural analysis of reinforced concrete beams strengthened with a cement based high strength composite material. Compos Struct 2011;94:143–55.
[8] Bencardino F, Carloni C, Condello A, Focacci F, Napoli A, Realfonzo R. Flexural behaviour of RC members strengthened with FRCM. state-of-the-art and predictive formulas. Compos: B - Eng 2018;148:132–48. https://doi.org/10.1016/j.compositesb.2018.04.051.
[9] Ebead U, Shrestha KC, Afzal MS, El Refai A, Nanni A. Effectiveness of fabric-reinforced cementitious matrix in strengthening reinforced concrete beams. J Compos Constr 2017;21:04016084.
[10] Alabdulhady Meyyada Y, Sneed Lesley H, Carloni Christian. Torsional behavior of RC beams strengthened with PBO-FRCM composite–an experimental study. Eng Struct 2017;136:393–405.
[11] Sneed Lesley H, Verre Salvatore, Carloni Christian, Ombres Luciano. Flexural behavior of RC beams strengthened with steel-FRCM composite. Eng Struct 2016;127:686–99.
[12] Gonzalez-Libreros Jaime Hernan, Sneed LH, D'Antino Tommaso, Pellegrino Carlo. Behavior of RC beams strengthened in shear with FRP and FRCM composites. Eng Struct 2017;150:830–42.
[13] Bellini A, Bovo M, Mazzotti C. Experimental and numerical evaluation of fiber-matrix interface behaviour of different FRCM systems. Compos B 2019;161:411–26.
[14] Raoof SM, Bournas DA. Bond between TRM versus FRP composites and concrete at high temperatures. Compos: Part B - Eng 2017;127:150–65.
[15] Triantafillou TC, Papanicolaou CG, Zissimopoulos P, Laourdekis T. "Concrete confinement with textile-reinforced mortar jackets. ACI Mater J 2006;103:28.
[16] Peled A. Confinement of damaged and nondamaged structural concrete with FRP and TRC sleeves. J Compos Constr 2007;11:514–22.
[17] Ombres L. Concrete confinement with a cement based high strength composite material. Compos Struct 2014;109:294–304.
[18] Trapko T. Effect of eccentric compression loading on the strains of FRCM confined concrete columns. Constr Build Mater 2014;61:97–105.
[19] Trapko T. Behaviour of fibre reinforced cementitious matrix strengthened concrete columns under eccentric compression loading. Mater Des 2014;54:947–54.
[20] Ombres L, Verre S. Structural behaviour of fabric reinforced cementitious matrix (FRCM) strengthened concrete columns under eccentric loading. Compos B 2015;75:235–49.
[21] Alabdulhady MY, Sneed LH, Abdelkarim OI, ElGawady MA. Finite element study on the behavior of RC beams strengthened with PBO-FRCM composite under torsion. Compos Struct 2017;179:326–39.
[22] Mazzucco G, D'Antino T, Pellegrino C, Salomoni V. Three-dimensional finite element modeling of inorganic-matrix composite materials using a mesoscale approach. Compos: Part B - Eng 2018;143:75–85.
[23] Grande E, Imbimbo M, Sacco E. Numerical investigation on the bond behavior of FRCM strengthening systems. Compos: Part B - Eng 2018;145:240–51.
[24] Kadhim MM, Adheem AH, Altaee MJ. Shear strengthening of RC beams with FRCM technique. Int J Eng Technol 2019;8:169–76.
[25] Trapko T. Confined concrete elements with PBO-FRCM composites. Constr Build Mater 2014;73:332–8.
[26] ANSYS. Release 17.2 Documentation for ANSYS. Version 17.2, ANSYS Inc., Canonsburg, PA, USA; 2016.
[27] ACI Committee 440.2R. Guide for the Design and Construction of Externally Bonded FRP Systems for Strengthening Concrete Structures. Detroit: American Concrete Institute; 2017.
[28] Mirmiran A, Zagers K, Yuan W. Nonlinear finite element modeling of concrete confined by fiber composites. Finite Elem Anal Des 2000;35(1):79–96.
[29] Teng JG, Xiao QG, Yu T. Three-dimensional finite element analysis of reinforced concrete columns with FRP and/or steel confinement. Eng Struct 2015;97:15–28.
[30] Abdallah MH, Shazly M, Mohamed HM, Masmoudi R, Mousa A. Nonlinear finite element analysis of short and long reinforced concrete columns confined with GFRP tubes. J Reinf Plast Compos 2017;36(13):972–87.
[31] Ghanem SY. Circular RC columns partially confined with FRP [Doctoral Dissertation]. USA: University of Kentucky; 2016. 10.13023/ETD.2016.124.
[32] Mirmiran A, Zagers K, Yuan W. Nonlinear finite element modeling of concrete confined by fiber composites. Finite Elem Anal Des 2000;35:79–96.
[33] Kent DC, Park R. Flexural members with confined concrete. J Struct Div 1971.
[34] Lam L, Teng J. Design-oriented stress–strain model for FRP-confined concrete. Constr Build Mater 2003;17:471–89.
[35] Kadhim MM, Adheem AH, Jawdhari A. Nonlinear finite element modelling and parametric analysis of shear strengthening RC T-beams with NSM CFRP technique. Int J Civ Eng 2019;17:1–12.
[36] ACI 318-14. Building code requirements for structural concrete and commentary. Farmington Hills (MI): American Concrete Institute; 2014, p. 519.
[37] Jawdhari A, Harik I. Simulation of delamination failures in RC Members strengthened with CFRP rod panels and CFRP laminates. ACI Special Publication N. 2018;327:5.1-5.20.
[38] Khan QS, Sheikh MN, Hadi MNS. Tension and compression testing of fibre reinforced polymer (FRP) bars. In: FRPRCS12 & APFIS2015 joint conference, Nanjing, China; 2015:1–6.